sciendo

TRANSACTIONS ON AEROSPACE RESEARCH
3(260) 2020, pp.30-48
DOI: 10.2478/tar-2020-0015
eISSN 2545-2835

NUMERICAL STUDY OF DETONATION PROCESSES IN ROTATING DETONATION ENGINE AND ITS PROPULSIVE PERFORMANCE

Tae-Hyeong Yi[1*], Jing Lou[2], Cary Kenny Turangan[2], Piotr Wolanski[3]
[1]Pukyong National University, 45, Yongso-ro, Nam-Gu, Busan, Republic of Korea
[2]Institute of High Performance Computing, 1 Fusionopolis Way, #16-16 Connexis, 138632 Singapore
[3]Łukasiewicz Research Network – Institute of Aviation, Al. Krakowska 110/114, 02-256 Warsaw, Poland
brianyi07@pknu.ac.kr • ORCID: 0000-0001-5358-3594
loujing@ihpc.a-star.edu.sg • ORCID: 0000-0003-0806-903X
cary@ihpc.a-star.edu.sg • ORCID: 0000-0003-3926-2369
piotr.wolanski@ilot.lukasiewicz.gov.pl • ORCID: 0000-0003-3963-7722

Abstract

Numerical studies on detonation wave propagation in rotating detonation engine and its propulsive performance with one- and multi-step chemistries of a hydrogen-based mixture are presented. The computational codes were developed based on the three-dimensional Euler equations coupled with source terms that incorporate high-temperature chemical reactions. The governing equations were discretized using Roe scheme-based finite volume method for spatial terms and second-order Runge-Kutta method for temporal terms. One-dimensional detonation simulations with one- and multi-step chemistries of a hydrogen-air mixture were performed to verify the computational codes and chemical mechanisms. In two-dimensional simulations, detonation waves rotating in a rectangular chamber were investigated to understand its flowfield characteristics, where the detailed flowfield structure observed in the experiments was successfully captured. Three-dimensional simulations of two-waved rotating detonation engine with an annular chamber were performed to evaluate its propulsive performance in the form of thrust and specific impulse. It was shown that rotating detonation engine produced constant thrust after the flowfield in the chamber was stabilized, which is a major difference from pulse detonation engine that generates repetitive and intermittent thrust.

Keywords: detonation wave, rotating detonation engine, propulsion, chemical kinetics, finite volume method, adaptive mesh refinement.

1. INTRODUCTION

Travel and transport information company OAG reported that for Asia Pacific, in January 2007, there were a total of 46,700 intercontinental flights and 493,000 intra-regional flights [1]. They are 9% and 7% higher, respectively, compared to January 2006. In 2002, there were only 29,000 flights to and from Asia Pacific, and 351,000 intra-regional flights. These statistics reflect the rapid growth of aviation industry globally, particularly in Asia Pacific with China and India leading the pack. Propulsion and power capabilities are pillars that support the current and future of commercial aircraft, which mould the aviation industry as well as establish the global conduit of commerce [2]. Among the most significant

development in terms of a revolutionary concept in a propulsion system is an engine based on unsteady detonation wave such as pulse detonation engine (PDE) [3, 4] and rotating detonation engine (RDE) [5, 6, 7, 8] owing to their higher propulsive efficiency, compared with deflagration-based conventional engines.

In a deflagration, the combustion wave travels at low subsonic speed, which is usually used in typical propulsion systems and power generations such as in aircraft and automobile engines, chemical technology and power engineering [4]. On the other hand, a detonation is a supersonic combustion in which chemical energy is instantaneously converted into thermal and kinetic energy of the reaction products behind its wave front. It is the most devastating form of gas or liquid explosions, and it does not require any obstructions of confinement for it to propagate at a supersonic speed. A velocity of 1.7-2.0 km/s and a pressure of 15-20 atm are typical in a hydrocarbon-air mixture at standard ambient conditions. The detonation wave is created by the interaction of a shock wave with the chemical reaction of a fuel-oxidizer mixture. The detonation wave can be initiated either directly or indirectly. While the direct initiation requires a large amount of energy such as using a very powerful spark plug, the indirect initiation may be achieved through a process of deflagration to detonation transition (DDT). In DDT, the acceleration of deflagration flame initiated by a weak spark is obtained by means of turbulence and then a shock wave is eventually formed. The shock wave compresses a fuel-oxidizer mixture, which strongly couples with a reaction zone. This process finally induces the detonation wave. The detonation, although very volatile and difficult to control, is a very attractive phenomenon regarding the thermodynamic efficiency of energy conversion, which lowers fuel consumption, compared to the deflagration.

For propulsion applications, detonation-based engines such as PDE and RDE offer higher engine efficiency, can be simple and compact owing to having fewer moving parts, and can operate over a wider range from take-off to supersonic speed [4]. It can be used as a pure propulsion system or as a hybrid with a turbine to deliver more thrust for minimal or no additional fuel consumption. The basic PDE cycle consists of four processes [3]: (a) filling a fuel-oxidizer mixture to a tube-type chamber, (b) initiating the detonation near a thrust wall, (c) detonation propagation through a chamber and (d) exhausting a burned gas and charging a cold ambient air through a blowdown process. Despite the advantages for a propulsion system, PDE development is still in preliminary stages due to several technical challenges, such as very loud noise it produces, large variation of thrust in time, material strength of the engine parts themselves, and how the intermittency of the detonation can be sustained for a long period of time.

By the beginning of this project in 2007, the development of detonation-based engines had been mainly focused on PDE that uses pulsating detonation waves propagating in a single or multiple long tube [4]. In addition to PDE, an alternative concept based on the detonation combustion for a propulsion system and power generation was introduced by Voitsekhovskii [9] and Nicholls [10] in the 1960s, namely the continuously RDE. Since the 2000s, it has been recognized as an alternative of PDE for a detonation-based engine due to the potential advantages of RDE [5-8, 11-15]. Compared with PDE, RDE provides significantly different engine operations [15]. While in PDE, the detonation propagates in the axial direction of a long tube-type chamber, RDE uses the detonation wave that continuously rotates in the azimuthal direction of an annular chamber, particularly a channel between inner and outer walls, shown in Fig. 1. A fuel-oxidizer mixture in RDE is continuously supplied and burnt by the rotating detonation located near an injection-wall. The PDE has a limited operating frequency because of the characteristics of its operating cycle such as purging and filling processes. However, RDE runs at very high frequency, typically several kHz [15]. Due to the inertia force of flowing-out burnt products, the combustion products are evacuated by themselves from the combustion chamber and the fuel-oxidizer mixture is constantly replenished to the chamber, which allows RDE to operate continuously. Whereas PDE requires a detonation initiation at each operating cycle, only a single initiation is required when starting RDE operation.

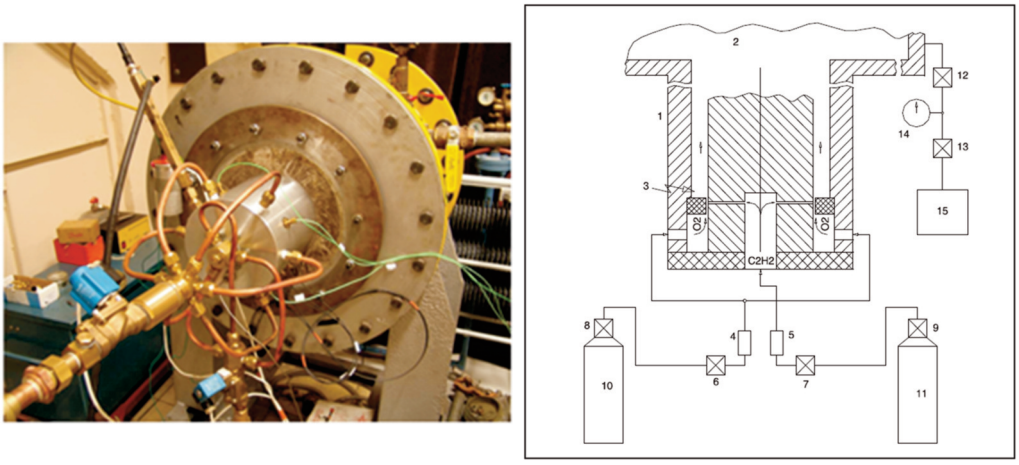

a) RDE with a short tube b) Schematic of an RDE test stand

Fig. 1. Experimental stand of the RDE conducted by Wolanski et al. [5]: 1 – detonation chamber; 2 – dump tank; 3 – spark plug; 4, 5 – flame stopper; 6, 7 – electromagnetic valves; 8, 9, 12, 13 – valves; 10 – O_2 supply bottle; 11 – C_2H_2 supply bottle; 14 – manometer; 15 – vacuum pump.

Because of its potential advantages, we proposed a collaborative research between the Institute of High Performance Computing (IHPC), Singapore and the Warsaw University of Technology (WUT), Poland in the development of RDE to provide a strong effort by combining the extensive experimental work at WUT and advanced modeling and numerical simulation tools at IHPC. The major research activity at WUT focused on RDE construction and its experimental analysis. The research scope at IHPC included: (a) the development of high-performance parallel, multi-dimensional codes with simple and detailed chemical kinetics, (b) modeling detonation phenomena in various combustion chambers, (c) model testing and verification via simulations, and (d) assisting the design optimization, which was aimed to improve the performance of rotating detonation engine.

Here we present the summary of several research achievements on the RDE development, conducted by IHPC in the cooperation project, particularly focused on examination of the flowfield structure in RDE and evaluation of its propulsive performance. For the work scheduled in the first year of this project, the main focus was on the building-up of the modeling methodology such as fuel injection conditions, geometric configuration and detonation initiation, which are the backbone of RDE modeling. These topics are described in Sections 2 and 3, where the detailed descriptions of governing equations with one- and multi-step chemical kinetics, numerical methods and RDE modeling are presented. In order to verify the code and the mechanism of one- and multi-step chemistries, the simulations of one-dimensional (1D) detonation wave propagating in a tube are performed in Section 4.1. These numerical results are compared with theoretical values obtained at Chapman-Jouguet (CJ) conditions. The flowfield structure in the RDE with two-dimensional (2D) rectangular and 3D annular chambers is described in Sections 4.2 and 4.4, respectively. In the 2D RDE chamber, moreover, the detailed cellular structure of the detonation wave is investigated with the multi-step chemical mechanism of a hydrogen-oxygen-argon (H_2-O_2-Ar) mixture in Section 4.3. The RDE with a 3D annular chamber is used to evaluate its propulsive performance in terms of thrust and fuel-based specific impulse. In the evaluation of propulsive performance, the one-step chemical mechanism of a hydrogen-air (H_2-air) mixture is used for numerical efficiency. In the last section, the concluding remarks and further works are summarized.

2. GOVERNING EQUATIONS AND CHEMICAL KINETICS

The governing equations considered in this study are 3D, unsteady Euler equations with source terms due to high-temperature chemical reactions. In this study, the chemical reactions of a fuel-oxidizer mixture are modeled with both one- and multi-step chemical mechanisms. Therefore, the governing equations are written in Cartesian coordinates in a vector form as:

$$\frac{\partial \vec{Q}}{\partial t}+\frac{\partial \vec{F}_x}{\partial x}+\frac{\partial \vec{F}_y}{\partial y}+\frac{\partial \vec{F}_z}{\partial z}=\vec{S}, \tag{1}$$

where the conservative variable vector $\vec{Q}$, the convective flux vectors $\vec{F}$ and the source vector $\vec{S}$ are respectively given in the next section, depending on which the chemical mechanism is used.

2.1. 3D Euler equations with one-step chemistry

When only gas-dynamics properties are considered to evaluate the propulsive performance of an engine, particularly in 3D simulations, a one-step, irreversible Arrhenius kinetics is suitable to save computational time. In this case, the flow and thermodynamic properties obey the law of a calorically perfect gas. Therefore, the conservative variable, convective flux and source vectors of the governing equations with one-step chemistry are written as:

$$\vec{Q}=\begin{bmatrix}\rho\\ \rho u\\ \rho v\\ \rho w\\ \rho E\\ \rho Y\end{bmatrix},\ \vec{F}_x=\begin{bmatrix}\rho u\\ \rho u^2+p\\ \rho uv\\ \rho uw\\ \rho uH\\ \rho uY\end{bmatrix},\ \vec{F}_y=\begin{bmatrix}\rho v\\ \rho uv\\ \rho v^2+p\\ \rho vw\\ \rho vH\\ \rho vY\end{bmatrix},\ \vec{F}_z=\begin{bmatrix}\rho w\\ \rho uw\\ \rho vw\\ \rho w^2+p\\ \rho wH\\ \rho wY\end{bmatrix},\ \text{and}\ \vec{S}=\begin{bmatrix}0\\ 0\\ 0\\ 0\\ 0\\ \dot{\omega}\end{bmatrix}, \tag{2}$$

where ρ is the density, p is the pressure, u, v and w are the velocity components, and Y is the mass fraction of reactant ($Y = 1$) or product ($Y = 0$). The total enthalpy H given in Eq. (2) is defined as:

$$H=E+\frac{p}{\rho}, \tag{3}$$

where the total energy E is the sum of the internal energy and kinetic energy, which is defined for the one-step chemistry as:

$$E=\frac{p}{(\gamma-1)\rho}+\frac{1}{2}\left(u^2+v^2+w^2\right)+qY. \tag{4}$$

Here, γ is the ratio of specific heats and q is the total chemical energy release. The mass production rate $\dot{\omega}$ in the source term is defined in the first-order Arrhenius form [15] by:

$$\dot{\omega}=-K\rho Y\exp\left(\frac{-E_a}{RT}\right), \tag{5}$$

where K is the pre-exponential factor, E_a is the activation energy, R is the specific gas constant and T is the temperature. The thermodynamic and chemical parameters in Eqs. (4) and (5) are given in Section 4.1.

2.2. 3D Euler equations with multi-step chemistry

Detailed multi-step chemistry of a hydrogen-based fuel-oxidizer mixture is coupled with the computational code such as:

$$\vec{Q}=\begin{bmatrix}\rho_i\\ \rho u\\ \rho v\\ \rho w\\ \rho E\end{bmatrix},\ \vec{F}_x=\begin{bmatrix}\rho_i u\\ \rho u^2+p\\ \rho uv\\ \rho uw\\ \rho uH\end{bmatrix},\ \vec{F}_y=\begin{bmatrix}\rho_i v\\ \rho uv\\ \rho v^2+p\\ \rho vw\\ \rho vH\end{bmatrix},\ \vec{F}_z=\begin{bmatrix}\rho_i w\\ \rho uw\\ \rho vw\\ \rho w^2+p\\ \rho wH\end{bmatrix},\ \text{and}\ \vec{S}=\begin{bmatrix}W_i\dot{\omega}\\ 0\\ 0\\ 0\\ 0\end{bmatrix}, \tag{6}$$

where ρ_i is the density of species i, W_i is the molecular weight of species i, and $\dot{\omega}_i$ is the mass production rate of species i. The chemical mechanisms of both H_2-air and H_2-O_2-Ar mixtures are extracted from GRI-Mech [16], and the overall reactions of their stoichiometric mixtures are given, respectively, as:

$$2H_2+O_2+3.762N_2\rightarrow 2H_2O+3.762N_2, \tag{7}$$

$$2H_2+O_2+7Ar\rightarrow 2H_2O+7Ar, \tag{8}$$

where nitrogen (N_2) and Ar are treated as diluent species. To obtain the chemical mechanism of the H_2-air or H_2-O_2-Ar mixture, an elementary reaction for the N_2 or Ar given in GRI-Mech [16] is added to the mechanism of the H_2-O_2 mixture [17], where it has 8 species and 27 elementary reactions, and third-body and pressure-dependent reactions are also included. For the detailed equations of the mass production rate, the specific heats, enthalpy and internal energy of species i, the reader can be referred to [18]. It is noted that in the multi-step chemistry, a thermally perfect gas is assumed, so that the specific heats, enthalpy and internal energy of species i are functions of the temperature only.

3. NUMERICAL METHODS

A detonation wave has complicated cellular structure, which comprises of a shock wave coupled with a reaction zone, triple points, shear layers and transverse wave, as shown in Fig. 2. When simulating the cellular structure of a detonation wave, which requires extremely high grid resolution in a very thin region, two major difficulties might arise from a wide range of spatial and temporal scales. For the former, an adaptive mesh refinement (AMR) approach using Paramesh [19] is employed by considering both the requirement of grid resolutions to capture a detonation front and numerical efficiency to save computational time. To take care of stiffness in time arisen from the latter, moreover, a time-operator splitting method [20] is used to decouple the governing equations into two steps: (1) homogeneous partial differential equations for the fluid dynamics and (2) ordinary differential equations with source terms due to chemical reactions.

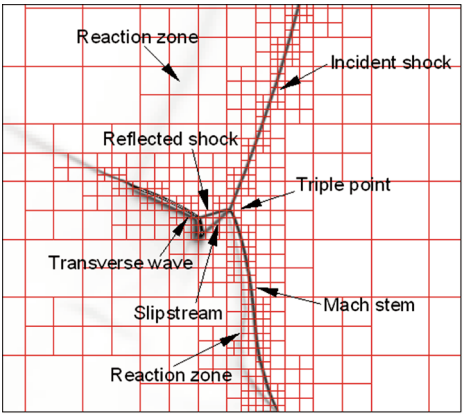

Fig. 2. Typical cellular structure of a detonation wave in a 2D rectangular domain. The squares in red color denote AMR blocks that have 20×20 grids.

3.1. Time-operator splitting method

In order to decouple the stiff source terms from the governing equations given in Eq. (1), a time-operator splitting method [20] is used whereby the equations are divided into two steps:

$$\begin{aligned} &\text{1st step:} \frac{\partial \vec{Q}}{\partial t} + \frac{\partial \vec{F}_x}{\partial x} + \frac{\partial \vec{F}_y}{\partial y} + \frac{\partial \vec{F}_z}{\partial z} = 0 \quad \left(\vec{Q}^n \Rightarrow \vec{Q}^{n+1/2}\right), \\ &\text{2nd step:} \frac{d\vec{Q}}{dt} = \vec{S} \quad \left(\vec{Q}^{n+1/2} \Rightarrow \vec{Q}^{n+1}\right). \end{aligned} \tag{9}$$

The first step is an intermediate stage that is solved with initial conditions, given from the preceding step. In the first step of Eq. (9), cell-centered finite volume method is employed for spatial discretization. The convective fluxes given in Eq. (9) at cell faces are approximated using the Roe scheme [21], where the left and right states are interpolated by the MUSCL approach [22] to obtain second-order accuracy in space. A minmod limiter function [23] is adopted to remove nonphysical oscillations around a discontinuity such as a shock wave. For temporal terms, the equations are integrated with second-order Runge-Kutta method. The second step of Eq. (9) is ordinary differential equations for chemical reactions, where its initial conditions come from the first step, which are given as $\vec{Q}^{n+1/2}$ in Eq. (9). For the one-step chemistry, it is solved using separation of variables [24]. Once the mass production rate $\dot{\omega}$ is solved, the temperature is then updated from the equation of state. For the multi-step chemistry, the second step becomes a system of ordinary differential equations, which are functions of the species density and temperature, solved using VODE [25].

In order to utilize an adaptive mesh approach in simulating the detonation wave, the code is coupled with an AMR package known as Paramesh [19]. Paramesh is an open-source code package written in Fortran 90 with Message-Passing Interface (MPI). It supports multi-dimensional models in a cartesian, cylindrical, spherical, or 2D polar coordinate system. The approach of Paramesh is based on the block structured AMR algorithm of Berger and co-workers [26], which builds a hierarchy of logically cartesian sub-grids.

3.2. Modeling of 2D and 3D RDEs

The physical and numerical setup of an RDE combustion chamber and its injection system described by Yi et al. [15] is summarized as follows. In RDE modeling, a fuel-oxidizer mixture is continuously supplied to the combustion chamber, depending on the location of the rotating detonation wave, through a large number of small injectors on the left-closed end. The products of detonation combustion are exhausted to the right open-end, where an aerospike nozzle or no nozzle is attached, as shown in Fig. 3(a). This configuration mimics the actual experimental setup of the RDE conducted by Wolanski et al. [5], one of which is shown in Fig. 1, where the annular chamber has a length of 177 mm, and inner and outer diameters of 130 and 150 mm, respectively. The RDE is started by the detonation wave tangentially transferred from an initiator. The 3D annular chamber can be simplified by assuming that the chamber channel becomes infinitely thin, so that the height of a 2D chamber is equal to the circumference of the annular chamber. Another assumption is that the inner and outer walls are required to be in adiabatic and flow-slip conditions. This simplified, 2D configuration is shown in Fig. 3(b).

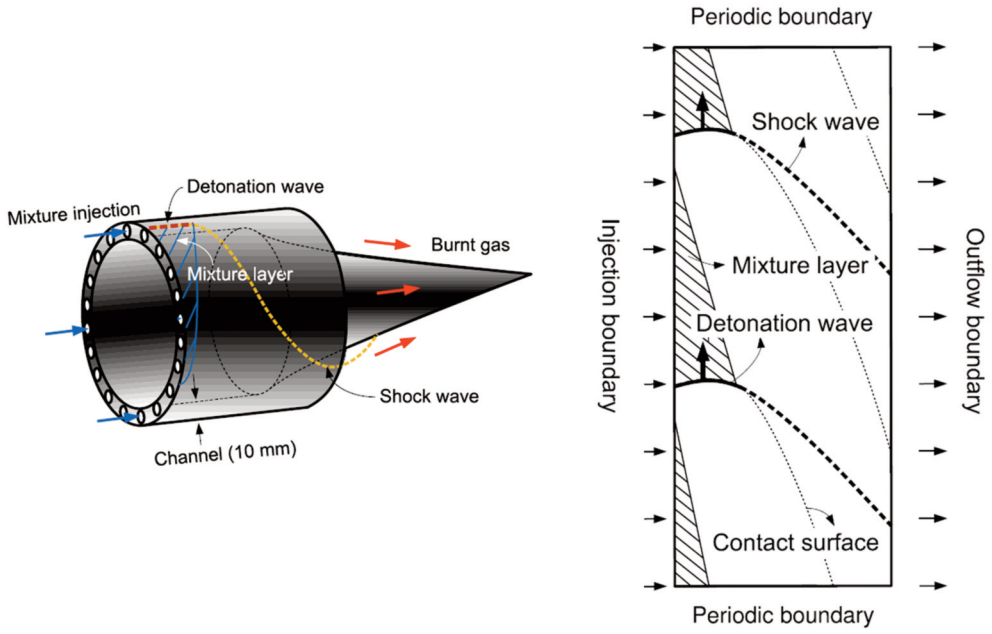

a) Annular chamber with an aerospike nozzle b) Simplified, 2D rectangular chamber [15]

Fig. 3. Schematic of an RDE chamber and its physical and numerical setup.

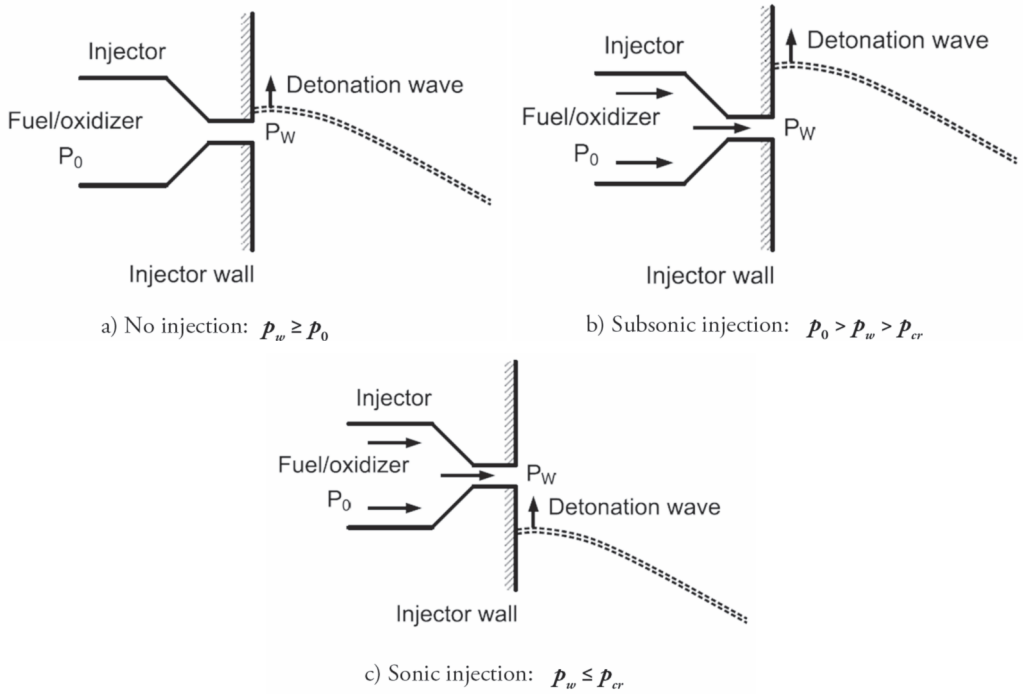

Fig. 4. Injection conditions based on the wall pressure in the front of an injector [15].

The operation of the RDE mainly depends on the incoming mass flow rate of a mixture [15], controlled by the injection conditions such as the total pressure and temperature of a mixture in the injector, and an injection area ratio. As described by Yi et al. [15], an injection system is modeled with three conditions, depending on the wall pressure in the front of an injector. The first condition is that the detonation wave is located just ahead of the injector, so that the injection-wall pressure is greater than the total pressure of the injectors and thus no injection occurs. The second is that it is less than the total pressure or greater than the critical pressure, which is obtained at the Mach number equal to unity. In this case, the detonation is propagating away from the injector. The last case is that the detonation is propagating far from or before the injector, so that it is less than the critical pressure. These injection conditions, actually determined by the location of the rotating detonation wave, are shown in Fig. 4 [15]. In the code, the pressure, temperature and axial velocity on the injection-wall boundary are expressed in terms of the convective fluxes, given in Eq. (2) or (6). The more detailed description and equations of modeling the injection system can be found in [15].

4. NUMERICAL RESULTS AND DISCUSSION

The in-house developed, multi-dimensional computational code has been verified with various test cases and applied for the simulations of detonation waves with the chemical kinetics of a hydrogen-based gas [15, 17, 19]. In [15, 19], the grid dependency with one- and multi-step chemistries on the simulations of RDE performance and the detonation cellular structure, respectively, were investigated to find out the proper grid resolutions in order to take account of numerical efficiency as well as accuracy. In this study, the H_2-air mixture is mainly adopted in 1D, 2D and 3D detonations, except a case for the cellular structure of the detonation in the 2D RDE, where a $2H_2+O_2+7Ar$ mixture is used. An argon dilution is chosen in this case because it tends to stabilize the detonation wave, so that the detonation with this mixture produces the cellular structure in a more regular form than a nitrogen dilution [27]. In 2D and 3D simulations, the total pressure of 10 atm and the total temperature of 300 K in the injector with the area ratio of 0.2 are applied for the injection boundary conditions, except as described.

4.1. Detonation propagation in a 1D chamber

The flow and thermodynamic properties of the 1D detonation wave obtained from numerical solutions, where the H_2-air mixture is modeled with one- and multi-step chemistries, are compared with theoretical values obtained from CEA [28]. A 1 m-long tube is used to ensure that an unsteady detonation wave is fully stabilized from an over-driven detonation at an initial stage. The detonation tube is modeled with AMR in 10 levels of refinement in which its initial grid is Δx = 0.003 m. The detonation is directly initialized with the high pressure and temperature (p = 20 atm and T = 2000 K) on the left-closed end of the tube filled with the H_2-air mixture at p = 1 atm, T = 300 K and V = 0 m/s. The finest grid is obtained by refining the grid around the front of the detonation wave, which is Δx = 0.0001 m. For the one-step chemistry of the H_2-air mixture, the thermodynamic and chemical parameters, where the calorically perfect gas is assumed, are adopted from Ma [29] as:

$$\gamma = 1.29,\ R = 368.9\ \text{J/kg}\cdot\text{K},\ K = 7.5\times10^{9}\,s^{-1} \text{ and } E_a = 4.794\times10^{6}\ \text{J/kg}. \tag{10}$$

The total chemical energy release q_0 is slightly modified to 2.8×10^6 J/kg for T = 300 K. With these parameters, the 1D detonation properties are compared in Fig. 5 with those of the multi-step chemistry. In the figures, the speed of the detonation wave obtained from the one-step chemistry is very close to that of the multi-step chemistry. The pressure and velocity of the detonation with both chemistries are in good agreement to each other as shown in Figs. 5(a) and (b). However, the temperature profile behind the detonation wave are slightly different, given in Fig. 5(c). This is the same in the density profile as given

in Fig. 5(d). Since the one-step chemistry uses a single value of the specific heat ratio, the density profile is also slightly different in the reactant.

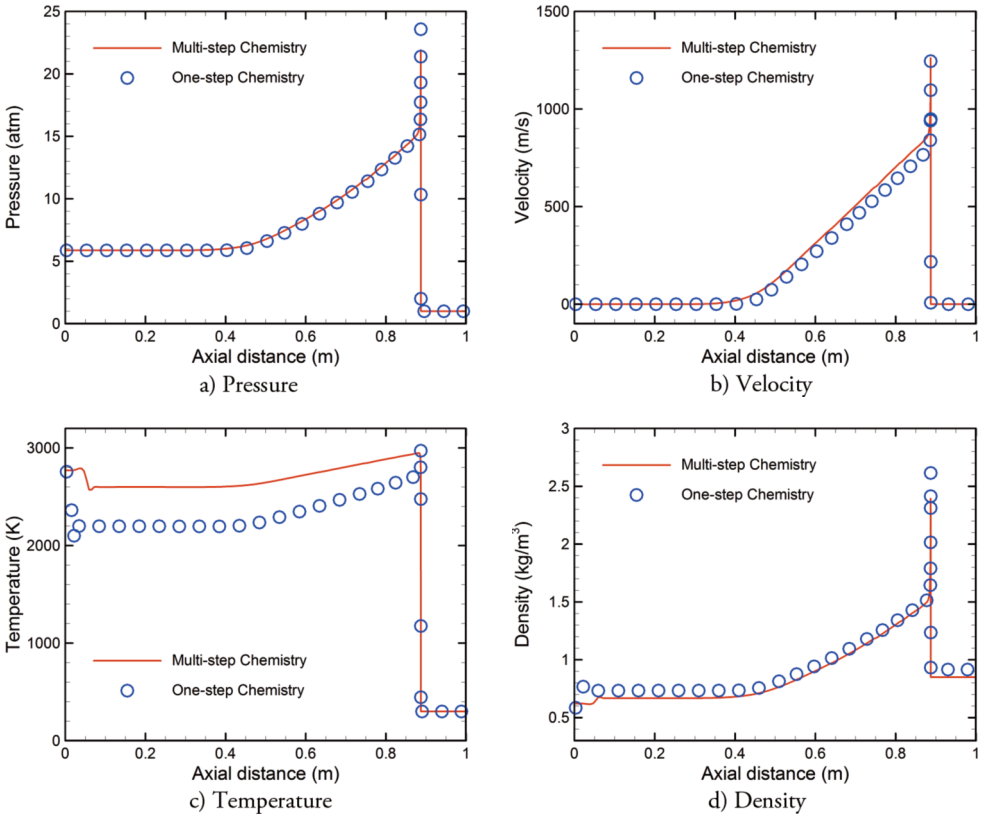

Fig. 5. Comparison of 1D detonation properties between the one- and multi-step chemistries of an H_2-air mixture at p = 1 atm and T = 300 K, captured at $t = 4.5 \times 10^{-4}$ s.

Tab. 1. Comparison of 1D CJ detonation properties between theoretical and numerical solutions.

Properties	Theory	Multi-step chemistry	One-step chemistry
U_D (m/s)	1979.3	1971.3	1971.0
p_{CJ} (atm)	15.08	15.04	16.14
T_{CJ} (K)	2956.1	2943.3	2753.8
Y_{CJ,H_2O}	0.2228	0.2230	–

The comparison of the detonation speed and the CJ properties obtained from the numerical solutions and theoretical values are listed in Table 1, where the theoretical values are computed with CEA [28]. The detonation speed and CJ properties obtained from the multi-step chemistry are very close to the theoretical values, which have the difference of 0.4% in the detonation speed (U_D), 0.27% in the CJ pressure (p_{CJ}), 0.43% in the CJ temperature (T_{CJ}), and 0.09% in the CJ mass fraction of H_2O (Y_{CJ,H_2O}). In this study, it is proved that the simulation with the one-step chemistry is possible to obtain the detonation CJ properties with acceptable accuracy (less than 7%) and describe the dynamics of detonation propagation at the accurate detonation speed. Therefore, it is still acceptable for evaluating of the propulsive performance of the RDE without affecting global performance trends.

In the work of Yi et al. [15], moreover, the 1D detonation wave with the one-step chemistry under various initial pressures and temperatures of the H_2-air mixture was investigated to verify the code by comparing with the theoretical CJ values. In the study, a maximum error less than 8% in both CJ pressure and temperature was achieved for the H_2-air mixture at p = 1 to 4 atm and T = 300 to 500 K.

4.2. RDE with a 2D rectangular chamber

The 2D RDE is modeled with a 0.177 m-long and 0.471 m-high rectangular chamber, which is a simplified version of the actual experimental RDE chamber [5]. Therefore, the height of a 2D domain is equal to the circumference of the actual chamber. The engine, partially filled by the H_2-air mixture near the injection-wall of the chamber, is started by the detonation wave tangentially transferred from an initiator. Therefore, the one-waved RDE is numerically modeled by placing a 1D, CJ detonation wave, which has the initial conditions of p = 1 atm and T = 300 K, in the left-bottom of the domain, so that the detonation wave propagates to the upper boundary near the injection-wall. Similarly, the two-waved RDE is initiated by placing two pieces of a 1D, CJ detonation wave into the left-bottom and left-middle of the domain, respectively, as shown in Fig. 6(a). These detonation waves propagate into the upper boundary and the combustion products move to the chamber exit, represented in Fig. 6(b). At this moment, the fresh mixture begins to be injected into the chamber. After one rotation, the triangular layers of the mixture are formed near the injection-wall as shown in Fig. 6(c). The shock waves emerged from the detonation waves and produced as a result of combustion propagate into the chamber exit. The flowfield in the RDE is stabilized after several rotations of the detonation waves.

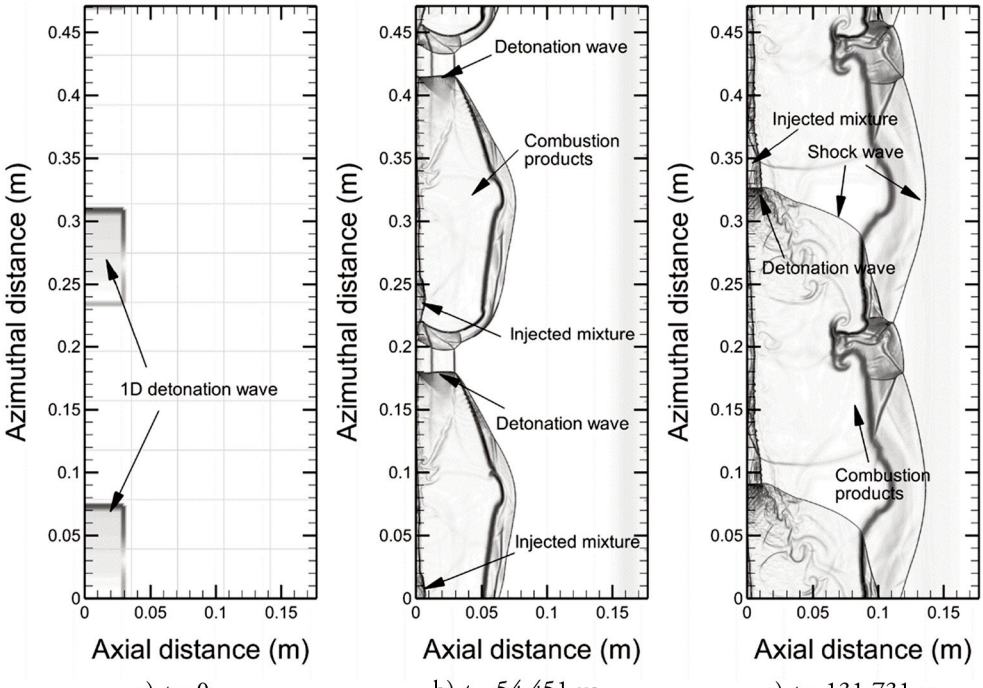

a) t = 0 s b) t = 54.451 μs c) t = 131.731 μs

Fig. 6. Time evolution of a flowfield in the two-waved RDE at initial stages, represented in the density gradient. In the left-most figure, the squares denote initial AMR blocks.

The detonation waves successively propagating around the circumference of the channel in the one- and two-waved RDE chambers are presented in Fig. 7, where the typical flowfield structure in the RDE chamber is shown in the density gradient after fully stabilized. As shown in Fig. 7, the flowfield in the RDEs is more complicated than that of PDE. While the fuel-oxidizer mixture is continuously injected from the injection-wall of the chamber, it is simultaneously burnt by the detonation wave propagating in the azimuthal direction. This forms a triangular layer of the fresh mixture. The mixture layer in the one-waved RDE is thicker than that of the two-waved RDE because the mixture is continuously flowing into the chamber axially between the successive detonation waves. As the result of the combustion product expansion, the non-reacting shock wave and contact surface are emerged from the right-end of the detonation wave. The combustion product is exhausting towards the chamber exit at near supersonic speed, depending on the back pressure. It is noted that in Fig. 7(a), the squares denote AMR blocks in which each block consists of 20×20 grids.

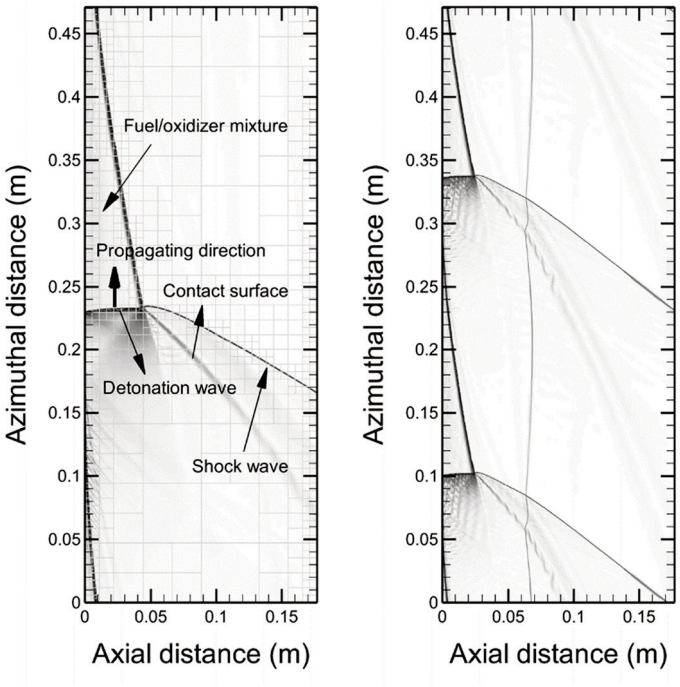

a) One-waved RDE b) Two-waved RDE

Fig. 7. Flowfield in the one- and two-waved RDEs with a 2D rectangular chamber, represented in the density gradient.

The detonation pressure distributions of the one- and two-waved RDE chambers, captured at x = 0.005 m near the chamber inlet are presented in Fig. 8. In the figure, the typical profile of a detonation wave is shown, such as a fuel-oxidizer mixture in the front of a detonation, a von Neumann pressure spike and a rarefaction wave behind a detonation front. The shock wave emanated from the right-end of the detonation wave is propagating into the chamber exit, indicated by as a wave discontinuity. These profiles are captured at x = 0.175 m along the azimuthal direction near the chamber outlet, where the average pressures of the one- and two-waved RDE are computed as 1.847 and 2.102 atm, respectively. In Fig. 9, the temperature at x = 0.005 m along the azimuthal direction is gradually decreased until

the expansion of the combustion product reaches the fresh mixture layer and then rapidly decreased to that of the fresh mixture. At x = 0.175 m near the chamber outlet, the average temperature of the two-waved RDE is rather higher than that of the one-waved RDE, which are computed as 1665 and 1508 K, respectively. As shown in Figs. 8(b) and 9(b), the pressure and temperature profiles of the two-wave RDE are symmetrical to the midpoint of the azimuthal direction.

Depending on the number of detonation waves resided in the chamber, the average value of flow and thermodynamic properties is rather different at the outlet. However, Yi et al. [15] reported that the thrust of the RDEs with different wave numbers eventually converges to a similar value.

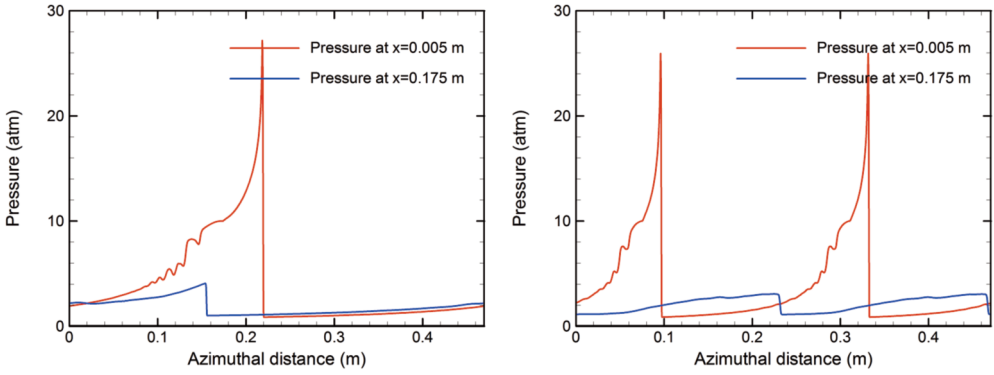

a) One-waved RDE b) Two-waved RDE

Fig. 8. Pressure profiles along the azimuthal direction at x = 0.005 and 0.175 m in the 2D RDEs.

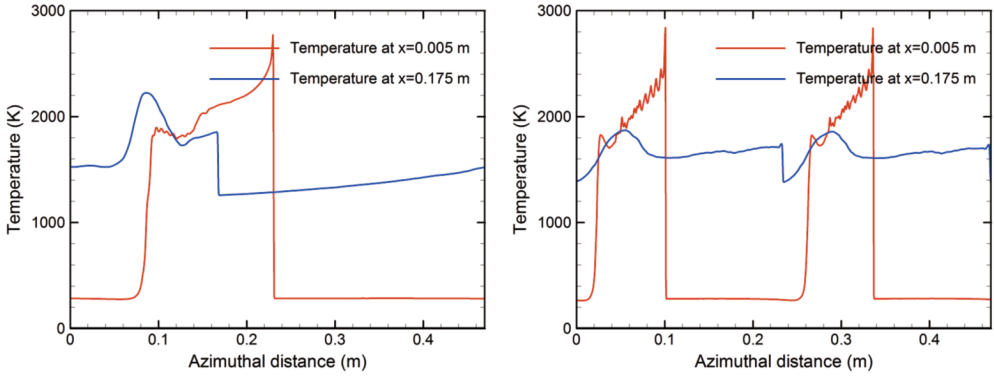

a) One-waved RDE b) Two-waved RDE

Fig. 9. Temperature profiles along the azimuthal direction at x = 0.005 and 0.175 m in the 2D RDEs.

4.3. Detonation cellular structure in 2D RDE

The cellular structure of the detonation wave in the one-waved 2D RDE chamber is studied with the $2H_2$+O_2+7Ar mixture and its density gradient is shown in Fig. 10(a). In this case, the detailed, multi-step chemical mechanism is used with 9 species and 28 elementary reaction steps. The 10-level refinement of AMR is applied to this simulation and thus the finest grid is obtained as $\Delta x = 1.56 \times 10^{-5}$ m around the front of the detonation. In this simulation, the total pressure and temperature of 7 atm and 450 K, respectively, are applied for the injection conditions to easily obtain the detonation cellular structure. One of the major features of the detonation wave in the RDE is that as shown in Fig. 10(a), it is curved

to the propagation direction since the mixture in the front of the detonation is non-uniform in the axial direction. The curved detonation wave in the RDE is also experimentally observed by Bykovskii et al. [7]. The pressure and temperature near the injection-wall in the front of the detonation, are about 0.74 atm and 418 K, respectively, and they are decreased to approximately 0.59 atm and 295 K around the front of the right-end of the detonation as shown in Fig. 10(b). The pressure and temperature increase in the deflagration area, where the fresh mixture layer and combustion products are interacted. Just before the end of the mixture layer, the detonation begins to degenerate into a non-reacting shock wave, where a reaction zone disappears. The detonation cellular structure that consists of incident shock, Mach stem, triple point, transverse wave and reaction zone is successfully captured in the figure. It is shown in Fig. 10(a) that the transverse waves in the middle region are much longer than those near the injection-wall.

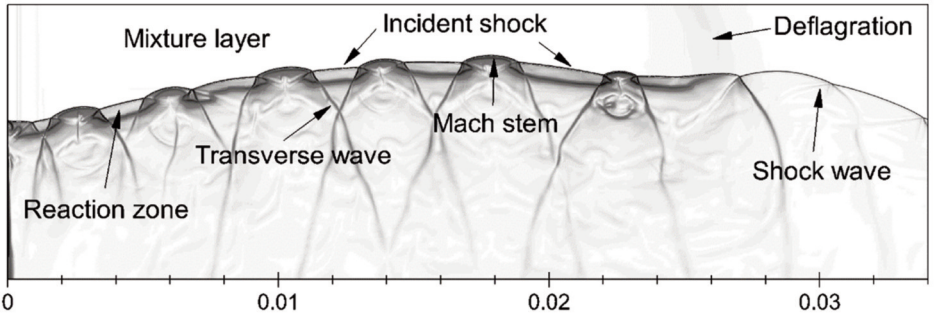

a) Detailed cellular structure of the detonation wave near the injection-wall of a chamber

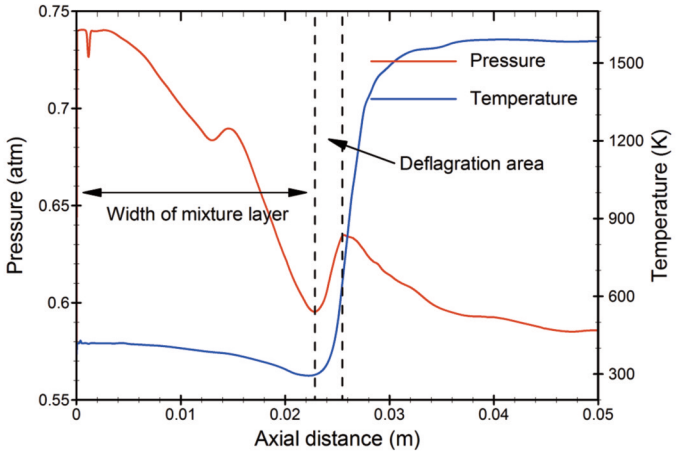

b) Mixture properties along the axial direction, captured at y = 0.0875 m

Fig. 10. Structure of the detonation wave and the mixture layer near the injection-wall of the one-waved RDE with a 2D rectangular chamber. The multi-step chemical mechanism of a $2H_2$+O_2+7AR mixture is used with 9 species and 28 reaction steps. Spatial unit is in meters.

4.4. RDE with a 3D annular chamber

The detonations continuously rotating in a 3D annular chamber with no nozzle are modeled in this section. The physical and numerical configuration is the same as those given in the 2D case. In addition,

the channel between the inner and outer walls of the annual chamber is 0.01 m high, as shown in Fig 3. The engine is started by placing the CJ detonation waves, which are obtained from the 1D simulation, in the azimuthal direction. The detonation waves are then stabilized after a few numbers of rotations and the triangular layers of a fuel-oxidizer mixture are properly formed. This moment is given in Fig. 11, where the pressure and axial velocity in the two-waved RDE are captured at $t = 3.1 \times 10^{-3}$ s. Figure 11(a) shows that the detonation pressure on the outer wall is slightly higher than that on the inner wall in the radial direction due to a centrifugal force. The combustion product is propagating into the chamber exit at the supersonic speed, given in Fig. 11(b). The axial velocity of the combustion product at the exit is ranged from approximately 850 to 1200 m/s, which corresponds to the Mach number of about 1.05 to 1.2. In the previous study [30], it was reported that the detonation waves propagate at approximately 1985 m/s after stabilized, so that the two-waved RDE is operated at the frequency of 8425 Hz.

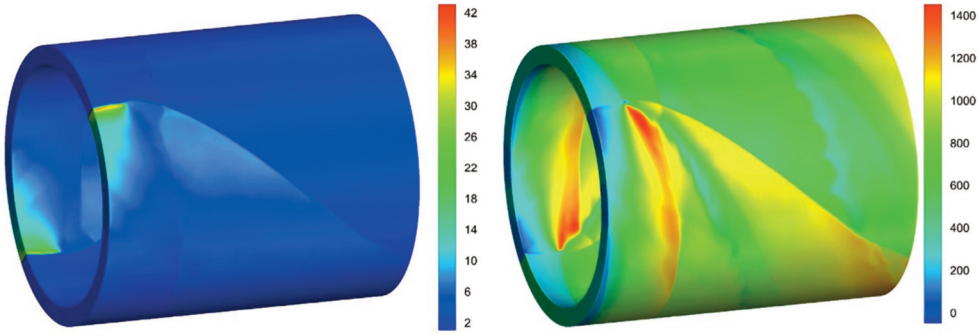

a) Pressure b) Axial velocity

Fig. 11. Flowfield of the two-waved RDE with a 3D annular chamber. The detonation waves propagating inside the channel are captured at $t = 3.1 \times 10^{-3}$ s.

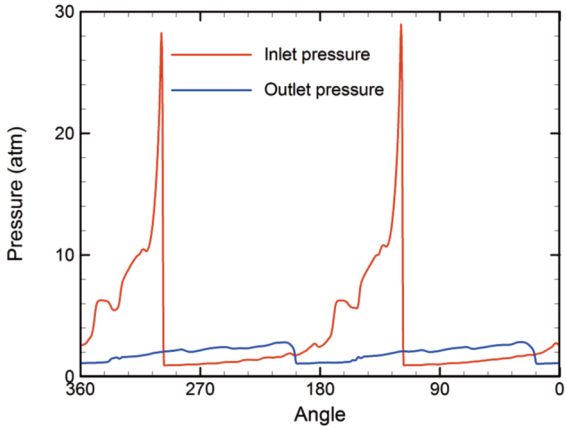

Fig. 12. Inlet and outlet pressure profiles along the centered line of the channel in a 3D annular chamber, captured at $t = 3.1 \times 10^{-3}$ s.

The pressure profiles along the centered line of the channel at the inlet and outlet are given in Fig. 12, where the typical profile of a detonation wave is also shown at the inlet. This is similar to that of the 2D case given in Fig. 8(b). At the outlet, the discontinuity in the pressure is a shock wave that is

emanating from the right end of the detonation and the average pressure is computed as 1.94 atm at the outlet. Figure 13 represents the temporal evolution of the pressures captured at x = 0.05 and 0.15 m on the outer wall up to $t = 3 \times 10^{-3}$ s. At initial stages, the pressures are much higher than that of the detonation wave. This is due to the interaction of the detonation wave with the combustion product generated by the preceding detonation. After about $t = 1.2 \times 10^{-3}$ s, the flowfield is stabilized and the pressures become almost constant, shown in Fig. 13.

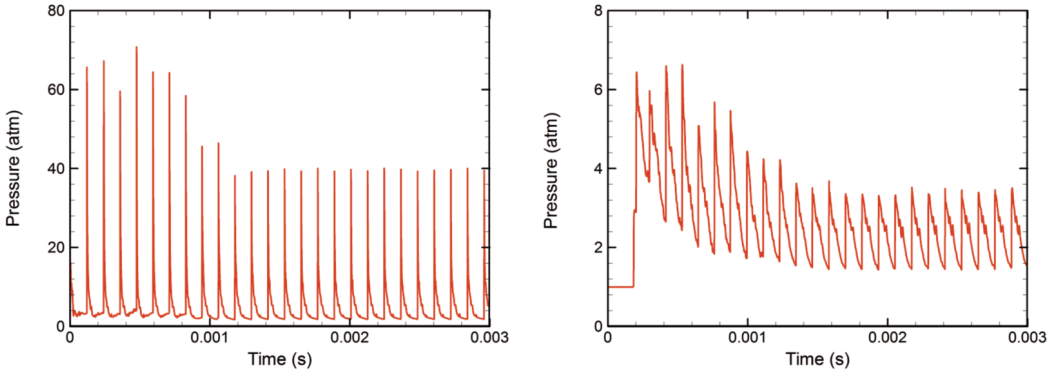

a) Pressure at x = 0.05 m b) Pressure at x = 0.15 m

Fig. 13. Temporal evolution of the pressure at x = 0.05 and 0.15 m on the outer wall of a 3D annular chamber.

The propulsive performance of the two-waved RDE with the annular chamber are evaluated in terms of thrust and fuel-based specific impulse. The thrust $F(t)$ is a change in momentum at the chamber exit [30], obtained as:

$$F(t) = \int_{exit} \left[pu^2 + (p - p_\infty) \right] dA, \tag{11}$$

where p_∞ is the ambient air pressure and A is the area of the chamber exit. The fuel-based specific impulse is a measure of engine efficiency and defined as the thrust per propellant weight [30], given by:

$$I_{st,f}(t) = \frac{F(t)}{g_0 \dot{m}_f}, \tag{12}$$

where g_0 is the gravity acceleration. In Eq. (12), the fuel-mass flow rate $\dot{m}_f$ is obtained from:

$$\dot{m}_f = \int \rho_f u \, dA, \tag{13}$$

where ρ_f is the fuel density.

The time variation of the thrust and fuel-based specific impulse of the two-waved RDE is plotted in Fig. 14 up to $t = 3 \times 10^{-3}$ s. After large variations, caused by the interaction between the detonation wave and its combustion product at initial stages, the thrust and fuel-based specific impulse produced by the RDE converge to the nearly constant values of 2.1 kN and 6.8×10^3 s, respectively, as shown in Fig. 14. This fact represents one of main advantages of RDE, compared with PDE that generates a repetitive and intermittent thrust due to blowdown and refilling processes. In the 2D simulation, it was demonstrated that RDE produces a total impulse higher than that of PDE [15].

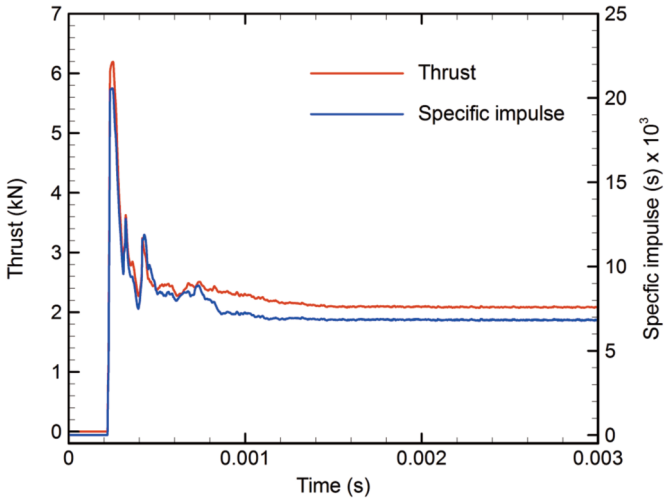

Fig. 14. Time variation of thrust and fuel-based specific impulse generated by the two-waved RDE with a 3D annular chamber up to $t = 3 \times 10^{-3}$ s.

5. CONCLUSIONS

In the three-year project, the research on modeling of detonation process in rotating detonation engine were divided into three phases: (1) code and model development, (2) model testing and verification via simulations, and (3) model implementations. Computational models developed in the first year was based on 3D Euler equations coupled with one- and multi-step chemical reactions. In order to take care of stiffness caused by high-temperature chemical reactions, time-operator splitting was used, which decouples the governing equations into homogeneous partial differential equations for the fluid dynamics and ordinary differential equations for the chemical reactions. For the partial differential equations, a finite volume approach with a MUSCL-based Roe scheme was employed for spatial discretization, while temporal terms were integrated by second-order Runge-Kutta method. Hydrogen-based fuel-oxidizer mixtures such as a H_2-O_2 mixture with N_2 or Ar diluents were modeled for this study and coupled with the computational code. For the multi-step chemistry, the reaction mechanism with 9 species and 28 elementary reaction steps was used for both mixtures. In the one-step chemistry, the constant thermodynamic and chemical parameters were given for the H_2-air mixture.

For model verification, the 1D detonation simulation with the one-step chemistry of the H_2-air mixture was compared with that of the multi-step chemistry. These numerical solutions were also compared with theoretical CJ detonation properties. The numerical solution with the multi-step chemistry was in very good agreement with the theoretical values, where the difference in the CJ detonation properties was less than 0.5%. However, the numerical solution with the one-step chemistry was slightly different from that of the multi-step chemistry and the theoretical values, in which the maximum error was less than 7%. In the 2D simulations, the detonation waves rotating in a rectangular domain were studied with both the one-step chemistry of a H_2-air mixture and the multi-step chemistry of a H_2-O_2-Ar mixture. The detailed flowfield structure observed in experimental works was successfully captured in the one- and two-waved RDEs. The flowfield structure in both cases consisted of a detonation wave propagating in the azimuthal direction, shock wave generated by combustion products, contact surface emanated from the right-end of the detonation wave, and the triangular layer of a fuel-oxidizer mixture that flows in the axial direction. Moreover, the profiles of

the pressure and temperature at the inlet and outlet of the one- and two-waved RDEs were presented to understand the characteristics of the flowfield in RDE. The cellular structure of the 2D detonation wave near the injection-wall of the one-waved RDE chamber was investigated with the H_2-O_2-Ar mixture. The typical cellular structure of the detonation wave, such as incident shock, Mach stem, transverse wave and reaction zone, was captured, except that the detonation wave was curved in the propagation direction and its transverse wave in the middle region was longer than those near the injection-wall. The simulation of the two-waved RDE with an 3D annular chamber was performed to evaluate its propulsive performance. The flowfield structure in the 3D RDE was quite similar to that of the simplified, 2D RDE, and so were the inlet and outlet pressure profiles. The operating frequency of the two-waved 3D RDE was obtained as 8425 Hz and it produced the constant thrust of 2.1 kN after stabilized, which was a major difference from PDE that generates a repetitive and intermittent thrust.

This study adopted the ideal model of an injection system that was based on the injection-wall pressure and supplied a premixed, stoichiometric fuel-oxidizer mixture to a chamber. In the future works, it is necessary to investigate the effects of various injection systems and chamber geometrics on the detonation wave propagation as well as the propulsive performance of RDE. Furthermore, the more realistic model of a simple fuel-oxidizer chemistry might be considered in 3D simulations.

Acknowledgements
The project was carried out at the Institute of High Performance Computing, A*STAR, Singapore (2006-2010), under the Singapore-Poland Science & Technology Co-operation agreement (IHPC/06-201802).

*Tae-Hyeong Yi – Formerly a Research Scientist, Fluid Dynamics, Institute of High Performance Computing A*STAR.

REFERENCES

[1] Press, O., 2007, "Asia Pacific's aviation industry remains buoyant as 85 million seats go on sale," www.oag.com.
[2] Sehra, A. K. and Whitlow, W., 2004, "Propulsion and power for 21st century aviation," Progress in Aerospace Sciences, vol. **40**, pp. 199-235.
[3] Bussing, T. and Pappas, G., 1994, "An introduction to pulse detonation engines," AIAA 1994-0263, https://doi.org/10.2514/6.1994-263.
[4] Roy, G. D., Frolov, S. M., Borisov, A. A., and Netzer, D. W., 2004, "Pulse detonation propulsion: challenges, current status and future perspective," Progress in Energy and Combustion Science, vol. **30**, pp. 545-672.
[5] Wolanski, P., Kindracki, J., and Fujiwara, T., 2006, "An experimental study of small rotating detonation engines," Pulsed and Continuous Detonation Ed., edited by Roy, G. D., Frolov, S. M., and Siniball, J., Torus Press, pp. 332-338.
[6] Wolanski, P., 2010, "Development of the continuous rotating detonation engines," Progress in Pulsed and Continuous Detonations, edited by Roy, G. D. and Frolov, S. M., Moscow, Torus Press, pp. 395-406.
[7] Bykovskii, F. A., Zhdan, S. A., and Vedernikov, E. F., 2006, "Continuous spin detonations," Journal of Propulsion and Power, vol. **22**(6), pp. 1204-1216.
[8] Lu, F. K. and Braun, E. M., 2014, "Rotating detonation wave propulsion: Experimental challenges, modeling, and engine concepts," Journal of Propulsion and Power, vol. **30**, pp. 1125-1142, https://doi.org/10.2514/1.B34802.
[9] Voitsekhovskii, B. V., 1960, "Stationary spin detonation," Soviet Journal of Applied Mechanics and Technical Physics, vol. **3**, pp. 157-164.

[10] Nicholls, J. A., Cullen, R. E., and Raglano, K. W., 1966, "Feasibility studies of a rotating detonation wave rocket motor," Journal of Spacecraft, vol. **3**, no. 6, pp. 893-898.
[11] Bykovskii, F. A., Zhdan, S. A., and Vedernikov, E. F., 2008, "Continuous spin detonation of hydrogen-oxygen mixtures. 1. Annular cylindrical combustors," Combustion, Explosion, and Shock Waves, vol. **44**, pp. 150-162.
[12] Daniau, E., Falempin, F., and Zhdan, S., 2005, "Pulsed and rotating detonation propulsion systems: first step towards operational engines," AIAA 2005-3233, https://doi.org/10.2514/6.2005-3233.
[13] Falempin, F. and Daniau, E., 2008, "A contribution to the development of actual continuous detonation wave engine," AIAA 2008-2679, https://doi.org/10.2514/6.2008-2679.
[14] Zhdan, S. A., Bykovskii, F. A., and Vedernikov, E. F., 2007, "Mathematical modeling of a rotating detonation wave in a hydrogen-oxygen mixture," Combustion, Explosion, and Shock Waves, Vol. **43**, No. 4, pp. 449-459.
[15] Yi, T.-H., Lou, J., Turangan, C. and Choi, J.-Y., and Wolanski, P., 2011, "Propulsive performance of a continuously rotating detonation engine," Journal of Propulsion and Power, vol. **27**, pp. 171-181, https://doi.org/10.2514/1.46686.
[16] Smith, G. P., Golden, D. M., Frenklach, M., Moriarty, N. W., Eiteneer, B. et al., GRI-Mech 3.0, http://combustion.berkeley.edu/gri-mech/
[17] Yi, T.-H., Lu, F. K., Wilson, D. R, Emanuel, G., 2017, "Numerical study of detonation wave propagation in a confined supersonic flow," Shock Waves, vol. 27, pp. 395-408, https://doi.org/10.1007/s00193-016-0666-8.
[18] Yi, T.-H., Anderson, D. A., Wilson, D. R., Lu, F. K., 2005, "Numerical study of two-dimensional viscous, chemically reacting flow," AIAA 2005-4868, https://doi.org/10.2514/6.2005-4868.
[19] MacNeice, P., Olson, K. M., Mobarry, C., deFainchtein, R., and Packer, C., 2000, "PARAMESH: A parallel adaptive mesh refinement community toolkit," Computer Physics Communications, vol. 126(3), pp. 330-354, https://doi.org/10.1016/S0010-4655(99)00501-9.
[20] Leveque, R. J., 2002, Finite Volume Methods for Hyperbolic Problems, Cambridge University Press.
[21] Roe, P. L., 1981, "Approximate Riemann solvers, parameter vectors and difference schemes," Journal of Computational Physics, vol. **43**, pp. 357-372.
[22] van Leer, B., 1979, "Towards the ultimate conservative difference scheme, V: A second-order sequel to Godunov's method," Journal of Computational Physics, vol. **32**, pp. 101-136.
[23] Tannehill, J. C., Anderson, D. A., and Pletcher, R. H., 1997, Computational Fluid Mechanics and Heat Transfer. Taylor and Francis, Washington, D. C.
[24] Williams, D. N., 2002, Numerical Modelling of Multidimensional Detonation Structure, Ph.D. thesis, University of Calgary, Calgary, Alberta.
[25] Brown, P. N., Byrne, G. D., and Hindmarsh, A.C., 1989, "VODE: A variable-coefficient ode solver, SIAM Journal on Scientific and Statistical Computing, vol. **10**, pp. 1038-1051.
[26] Berger, M. and Oliger, J., 1984, "Adaptive mesh refinement for hyperbolic partial differential equations," Journal of Computational Physics, vol. **53**, pp. 484-512.
[27] Lee, J. H. S., 2008, The Detonation Phenomenon, Cambridge Univ. Press, New York.
[28] Gordon, S. and McBride, B. J., 1976, "Computer program for calculation of complex chemical equilibrium compositions and application I. Analysis," Tech. Rep. NASA RP-1311.
[29] Ma, F., Choi, J. Y., and Yang, V., 2005, "Thrust chamber dynamics and propulsive performance of single-tube pulse detonation engines," Journal of Propulsion and Power, Vol. **21**, No. 3, pp. 512-526, https://doi.org/10.2514/1.7393.
[30] Yi, T.-H., Turangan, C., Lou, J., Wolanski, P., Kindracki, J., 2009, "A three-dimensional numerical study of rotational detonation in an annular chamber," AIAA paper 2009-0634, https://doi.org/10.2514/6.2009-634.

BADANIE NUMERYCZNE PROCESÓW DETONACJI W WIRUJĄCYM SILNIKU DETONACYJNYM I JEGO WYDAJNOŚCI NAPĘDOWEJ

Abstrakt

Przedstawiono badania numeryczne propagacji fali detonacyjnej w wirującym silniku detonacyjnym oraz jego wydajności pędnej z jedno- i wielostopniową mieszanką chemiczną na bazie wodoru. Kody obliczeniowe opracowano w oparciu o trójwymiarowe równania Eulera w połączeniu z pojęciami źródłowymi, które obejmują wysokotemperaturowe reakcje chemiczne. Obowiązujące równania zostały zdyskredytowane przy użyciu metody skończonej objętości opartej na schemacie Roe'a dla terminów przestrzennych oraz metody Runge-Kutta drugiego rzędu dla terminów czasowych. W celu weryfikacji kodów obliczeniowych i mechanizmów chemicznych przeprowadzono jednowymiarowe symulacje detonacji z jedno- i wieloetapowymi chemikaliami mieszaniny wodoru i powietrza. W symulacjach dwuwymiarowych badano fale detonacyjne obracające się w komorze prostokątnej w celu zrozumienia jej charakterystyki pola przepływu, gdzie udało się uchwycić szczegółową strukturę pola przepływu zaobserwowaną w doświadczeniach. Przeprowadzono trójwymiarowe symulacje dwufalowego wirującego silnika detonacyjnego z komorą pierścieniową w celu oceny jego właściwości pędnych w postaci ciągu i impulsu właściwego. Wykazano, że wirujący silnik detonujący wytwarza stały ciąg po ustabilizowaniu się pola przepływu w komorze, co stanowi istotną różnicę w stosunku do silnika detonującego impulsowo, który wytwarza powtarzalny i przerywany ciąg.

Słowa kluczowe: fala detonacyjna, wirujący silnik detonujący, napęd, kinetyka chemiczna, metoda skończonej objętości, adaptacyjne udoskonalanie siatki.